Mechanical and Water Absorption Properties of Short Banana Fiber/Unsaturated Polyester/Molecular Sieves + ZnO Nanorod Hybrid Nanobiocomposites

Chinnappa Arumugam, Gandarvakottai Senthilkumar Arumugam, Ashok Ganesan, and Sarojadevi Muthusamy*

ACCESS | Metrics & More | Article Recommendations

ABSTRACT: ZnO nanorods were prepared by the sol−gel method and characterized using UV−visible absorption spectroscopy, Fourier transform infrared (FT-IR) spectroscopy, powder X-ray diffraction (PXRD), thermogravimetric analysis/differential thermogravimetry (TGA/DTG), high-resolution transmission electron microscopy (HR-TEM), field emission scanning electron microscopy (FE-SEM), and energy-dispersive X-ray spectroscopy (EDAX). Banana fiber/polyester resin (BF/PE) biocomposites and BF/PE/MS/nano ZnO nanobiocomposites were made using the untreated and chemically treated (with NaOH, formic acid, acetic anhydride, hydrogen peroxide, and potassium permanganate) banana fiber (BF), unsaturated polyester resin (PE), molecular sieves (MS), and the prepared ZnO nanorods. The $KMnO_4$, Ac_2O, and NaOH treatments enhanced the thermal stability of the nanobiocomposites. Addition of 2% of ZnO nanorods increased the tensile strength of all of the chemically treated BF/PE/MS biocomposites. The chemical treatments alone decreased (NaOH—15.4 MPa; $KMnO_4$—14.5 MPa; H_2O_2—9.9 MPa; Ac_2O—7.9 MPa; HCOOH—6.9 MPa) the compressive strength of the untreated BF/PE/MS biocomposite (25.9 MPa). But the chemical treatment and addition of ZnO nanorods enhanced the compressive strength effectively (48.5, 41.6, 39.4, 37.0, and 34.6 MPa for NaOH, HCOOH, $KMnO_4$, H_2O_2, and Ac_2O treatments, respectively) compared to the untreated BF/PE/MS biocomposites (24.0 MPa). The H_2O_2 (69.0 MPa) and NaOH (62.9 MPa) treatments enhanced the flexural strength of the untreated BF/PE biocomposites (51.6 MPa). The addition of ZnO nanorods enhanced the flexural strength of all of the chemically treated (except NaOH) BF/PE/MS biocomposites (55.7, 59.4, 79.0, and 67.4 MPa for HCOOH, Ac_2O, H_2O_2, and $KMnO_4$ treatments, respectively). The impact strengths of the biocomposites were enhanced by both chemical treatments and addition of ZnO nanorods. The addition of ZnO nanorods decreased the water absorption of the biocomposites significantly from 24.3% for the untreated to a minimum of 14.5% for the H_2O_2-treated BF/PE/MS/ZnO nanobiocomposite.

1. INTRODUCTION

In the last few decades, natural fibers have gained increasing importance and usage due to their ability to replace synthetic fibers in composites applications. They possess attractive properties such as low cost, low density, and high specific strength/stiffness.[1] In addition to these reasons, they are renewable and their production requires little energy and involves CO_2 absorption, and return of oxygen to the environment.[2] Many authors reported the use of natural fibers such as sisal, banana, henequen, jute, hemp, and wood pulp as reinforcements in polymer matrices.[3−8] The extensive supply of natural fibers and the versatility to enhance their properties by surface treatments make these fibers an ideal alternative to conventional synthetic reinforcements. In the last few decades, the natural cellulose fiber-reinforced composite materials have been increasingly used in various automotive applications by a number of automotive companies, construction industry,

sports, aerospace, and other sectors, such as window frame panels, roofing, and bicycle frames.[9−12] Because of the hydrophilic nature of the plant fibers, they are incompatible with the hydrophobic organic polymers and they form composites with poor interfacial bonding and poor mechanical properties. Chemical treatment of natural fibers is an important method to be adopted in the production of their composites to improve their mechanical properties and reduce water absorption. It was found that the hydroxyl groups in the
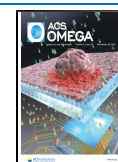
cellulosic fibers are either removed or modified to less hydrophilic or hydrophobic groups by different chemical treatments, which minimize the overall hydrophilic nature of the fibers and improve the mechanical strength as well as the dimensional stability of natural fiber-reinforced polymer composites. The effects of various chemical treatments on cellulose fibers, which were used as reinforcements for thermoplastics and thermosets, were studied.[13] Composite materials are the most adaptable engineering materials with the perfect combination of two different components, natural/synthetic fibers as reinforcement and polymer matrix with the perfect physical or chemical properties of each component.[14] Natural fiber-reinforced hybrid polymer composites provide designers with the ability to customize composites at a low cost that cannot be accomplished in binary structures with a single fiber/filler dispersed in the matrix.[15] Hybridization is a method of incorporation of two different reinforcements (either synthetic fibers/nanofillers/natural/metallic fibers in one polymer matrix) or the incorporation of single reinforcement in polymer blends, to produce better properties such as high mechanical properties, thermal stability, and reduced water absorption properties, which cannot be realized in conventional composite materials.[16,17] Hybrid materials are technologically advanced composite materials composed of two or more separate components at the molecular or nanometer level. They have improved tensile, compressive, and impact properties.[18] The properties of hybrid composites made using two different fibers are controlled solely by the length, direction, and type of the fibers, the degree of intermingling of the fibers, the arrangement of the fibers, and the bonding of the fibers with the resin. Researchers concluded from their analysis that the addition of a very small amount of nanoparticles to the matrix can significantly boost the properties, without affecting the weight or processability of the natural fiber-reinforced composites. So far, many pioneering works have been performed on natural fiber hybrid nanocomposite materials using nanoparticles for a variety of advanced applications.[17,19]

Nanofillers, either from natural or synthetic sources, are therefore of great interest and are considered to be the most promising materials of the future due to their specific properties compared to bulk counterparts. The most popular nanofillers include carbon nanotubes, layered nanoclays, nanofibers, ultradispersed diamonds (nanodiamonds), inorganic nanotubes, fullerenes, nanometal oxides, calcium carbonate, metallic nanoparticles, POSS, and graphite.[20,21] The application of nanofillers greatly enhances or changes the variable properties of materials, including physical, mechanical, electronic, electrical, and thermal properties, often in combination with natural or unconventional fillers.[22,23] Inorganic and organic nanofillers have gained significant attention due to their peculiar properties and various possible applications in the aerospace, automotive, electronics, and construction industries.[24,25] Banana is cultivated in India extensively, and the fibers can be extracted from the wastes after the fruits are removed. Banana fibers obtained from the dried stalk of banana trees, a waste product of banana production, offer possibilities for engineering applications, including automotive applications. Banana fibers consist of approximately 35% cellulose, 15% hemicellulose, 20% lignin, 10% moisture, and 20% of waxy and other extractives. The relatively large quantity of crystalline cellulose phase imparts high structural strength to the banana fiber. Banana fiber has

reasonably good basic strength properties[26−28] and lower density than glass fibers.[29] Hence, several authors have studied the possibilities for the making of banana fiber-reinforced polymer composites. Also chemical treatment of the fiber and addition of nanoclay were reported to improve the mechanical and thermal properties of its composites with epoxy resin.[30]

In this study, it is proposed to study the effect of chemical treatment of the short banana fibers with different chemicals like alkali, formic acid, acetic anhydride, hydrogen peroxide, and potassium permanganate and the addition of microsized inorganic fillers, namely, zeolite and ZnO nanorods, on the mechanical and thermal properties of the hybrid nano-biocomposites with unsaturated polyester resin. The aim of this research work is to improve the mechanical properties and reduce the percentage of water absorption.

2. EXPERIMENTAL SECTION

2.1. Materials. The banana fiber used in the present study was obtained from Sri Achu Fibres, Erode, Tamilnadu, India. The banana fibers were hand-chopped to an average length of 2 cm. The general-purpose unsaturated orthophthalic polyester resin (GP Resin—0051MNP), the standard laminating system in the composites industry, and methyl ethyl ketone peroxide (MEKP) and cobalt octoate, catalyst and accelerator, respectively, were obtained from Covai Seenu & Company, Coimbatore, Tamilnadu, India. Zinc sulfate ($ZnSO_4 \cdot 7H_2O$), hydrogen peroxide (H_2O_2), and triethanolamine (TEA) were purchased from Merck, Mumbai. Methanol, sodium hydroxide, formic acid, acetic anhydride, potassium permanganate, and glacial acetic acid were purchased from SRL Chemicals (P) Ltd., Mumbai, and were of analytical grade. Acetone was obtained from Moly Chemicals (P) Ltd., Mumbai. Molecular sieves ($4A^0$) were obtained from Fisher Scientific, Mumbai.

2.2. Measurements. Ultraviolet−visible (UV−vis) absorption spectra of ZnO nanorods were measured with a PerkinElmer Lambda 750 UV−vis spectrophotometer in the range of 190−1100 nm. The powder sample was dispersed in methanol, and the spectrum was recorded using a 10 mm quartz cell at 25 °C. Fourier transform infrared spectra were measured for dry powder after making pellets with KBr on a BRUKER VECTOR 22 FT-IR spectrophotometer operating from 400 to 4000 cm^{-1}. Powder X-ray diffraction (PXRD) pattern of ZnO nanorod was recorded using a PANalytical X'pert PRO diffractometer with Cu Kα radiation (1.54 A^0), the Netherlands. The ZnO nanorod was scanned in the 2θ range of 20−100°. All of the peaks were assigned and compared with the database published by the Joint Committee on Powder Diffraction Standards (JCPDS). Thermogravimetric analysis (TGA) of the ZnO nanorod and all of the composite samples were obtained with a PerkinElmer TGA/DTA 6300 at a heating rate of 5 °C min^{-1} in ambient air. The morphology of the ZnO nanorod sample was measured using scanning electron microscopy (SEM), and energy-dispersive X-ray (EDAX) analysis was performed in an FE-SEM JSM-7100F JEOL instrument. For measurements, the ZnO nanorod powder sample was drop-cast on the glass and fiber samples were fixed at a carbon tap and dried under vacuum. All of the samples were gold-coated before starting the measurement. High-resolution transmission electron microscopy (HR-TEM) images were measured using an FEI Technai G2 12 Twin TEM 120 keV transmission electron microscope. A diluted solution was drop-cast on the carbon-coated copper grid and was dried under vacuum. Images were collected at 120 keV.
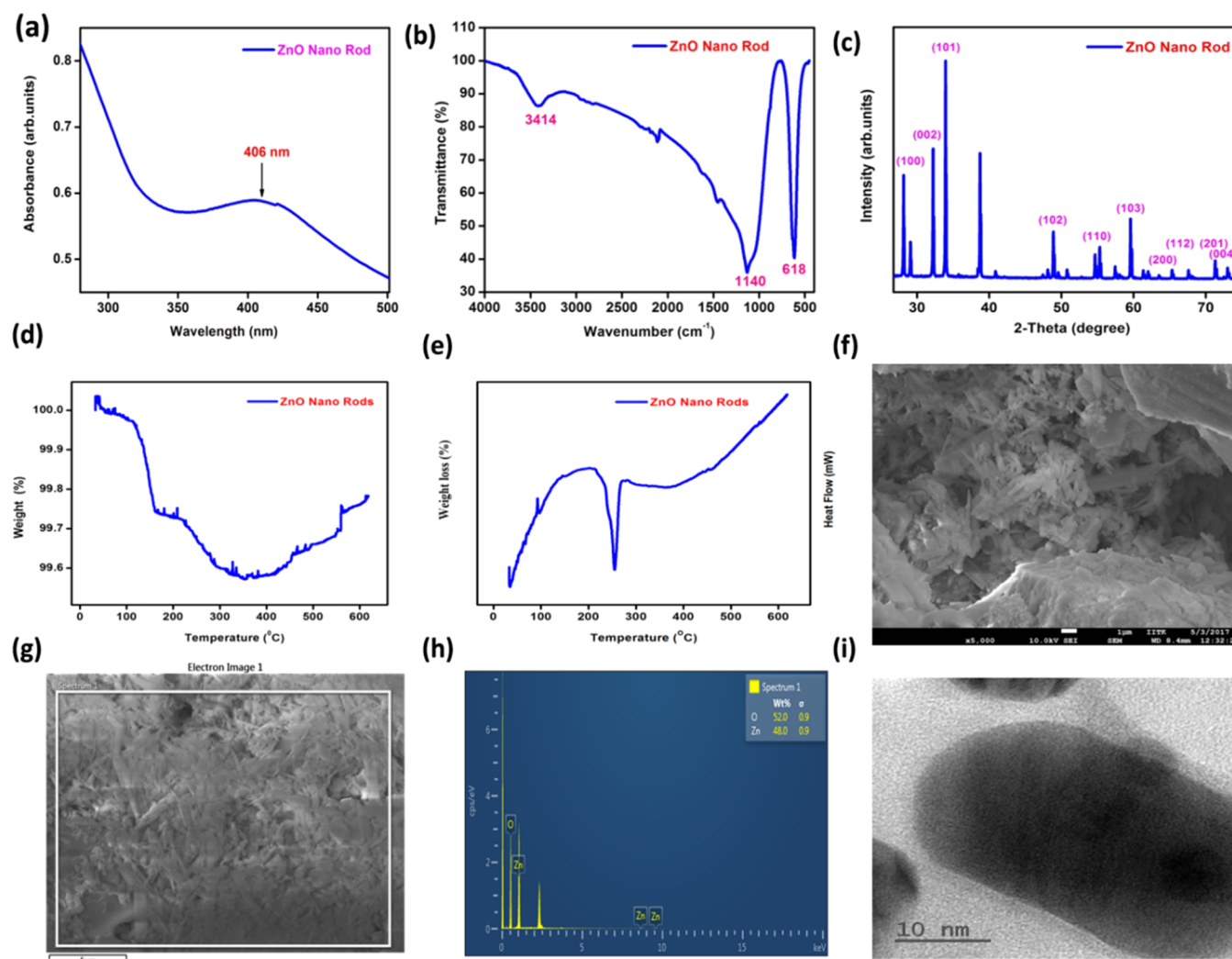
Figure 1. Characterization of ZnO nanorods. (a) UV−visible absorption spectrum, (b) Fourier transform infrared (FT-IR) spectrum, (c) powder XRD pattern, (d) TGA curve, (e) differential thermogravimetry (DTG) curve, (f) field emission scanning electron microscopy (FE-SEM) image, (g) FE-SEM-EDX image, (h) FE-SEM-EDX curve, and (i) high-resolution transmission electron microscopy (HR-TEM) image.

3. RESULTS AND DISCUSSION

3.1. Synthesis and Characterization of ZnO Nanorod.

3.1.1. Synthesis of ZnO Nanorods. During the previous three decades, few hundreds of papers have been published on the various possible methods of synthesis (including sol−gel method) and characterization of ZnO nanoparticles.[31,32] Different ZnO nanoparticle morphologies have been reported that include flower-like ZnO,[33,34] spherical ZnO,[35] and elliptical ZnO.[36] A thorough analysis of the literature reveals that in aqueous medium containing Zn^{2+} and OH^- ions, different species form as a function of pH. ZnO is mainly formed at pH values between 9 and 13, whereas $Zn(OH)_2$ predominated at pH 6.0−9.0. It was reported that one of the accelerators of ZnO formation is the presence of excess NaOH (or alkaline conditions) during precipitation. The use of a large excess of one reactant to the other and allowing a certain exposure time may be inferred to be another ZnO formation accelerator.[37] Also, the Zn^{2+} ion is known to bind with bases like ethylene diamine, triethanolamine (TEA), lysozyme, etc. and form complexes, thereby controlling the hydrolysis of the zinc hydroxide into ZnO.[38,39] TEA $[N(CH_2-CH_2-OH)_3]$, being a complexing agent, coordinates to zinc ions and forms

complex with Zn^{2+}, thereby enhancing the conversion of zinc hydroxide into ZnO that gets adsorbed on the ZnO surface, resulting in the enhancement or inhibition of the growth of ZnO crystals along different planes. The TEA content influences the morphology of the ZnO nanoparticles formed significantly.[40] Ban et al.[41] reported the preparation ZnO crystals using zinc sulfate heptahydrate, TEA, and tetramethyl ammonium hydroxide (TMAH) as zinc source, stabilizer, and base source, respectively, in water, at 0.2 mol L^{-1} of Zn and TEA/Zn = 4. They suggested that the zinc species was dissolved as zincate ions $Zn(OH)_3^-$ and $Zn(OH)_4^{2-}$ (but the solubility is very low)

$$Zn^{2+} + 2OH^- \rightarrow Zn(OH)_2\downarrow$$

$$Zn(OH)_2 + OH^- \rightarrow [Zn(OH)_3]^-$$

$$Zn(OH)_2 + 2OH^- \rightarrow [Zn(OH)_4]^{2-}$$
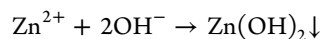
and that the stabilization of zincate ions with TEA enabled the solution with high Zn concentration. Zincate ions react with TEA as follows

$$[Zn(OH)_3]^- + TEA - H_3 \leftrightarrow [Zn(TEA)]^- + 3H_2O$$

and

$$[Zn(OH)_4]^{2-} + TEA - H_3$$
$$\leftrightarrow [Zn(OH)(TEA)]^{2-} + 3 H_2O$$
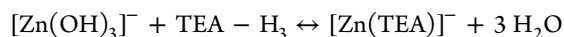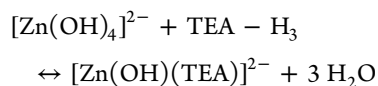
A coordinate bond was expected to be formed between the N atom in the coordinated TEA ligand and the Zn atom, resulting in stable complex ions, which decompose on heating to form ZnO crystals. They also reported the formation of hexagonal rod-shaped crystals at high TMAH/Zn ratios (highly basic media).[41]

It has been reported with enough experimental evidence that with a very high TEA content, the growth of the crystals along the 0001 plane is inhibited and hence the aspect ratio of the nanoparticles formed decreases, while with lower TEA contents, the crystal growth along the 0001 plane is enhanced, leading to the formation of long rodlike crystals. Based on these observations, in the present work, a sol−gel method using zinc sulfate, triethanolamine (to induce the particle growth with the nanorod morphology) sodium hydroxide, ethanol, and water was adopted for the preparation of the ZnO nanorods. A large excess (2.5 mol) of sodium hydroxide was used to facilitate the quick conversion of the $Zn(OH)_2$ formed into ZnO. A lower quantity (0.12 mol) of TEA was used to control the ZnO nanoparticle formed to have the morphology of the nanorod (Figure 8). The formation of the ZnO nanostructures is a complex process and mostly considered to include three main steps: formation of the hydroxide in the gel form, generation of ZnO nuclei, and subsequent ZnO crystal growth. The $[Zn(OH)_4]^{2-}$ complexes serve as basic growth units for the preparation of ZnO nanostructures.[40,41] Based on the intense scrutiny of the literature, the mechanism of the formation of ZnO nanorods in the present work is also proposed to be similar to the one mentioned above. It is believed that the presence of low concentrations of TEA facilitates the formation of ZnO with nanorod morphology as reported in the literature.[38,40]

3.1.2. UV−Visible Spectrum of ZnO Nanorods. The optical properties of ZnO nanorods were characterized using a UV−visible spectrophotometer. The UV−visible absorption spectrum of ZnO nanorod is shown in Figure 1a. The absorption peak (λ_{max}) near 406 nm confirms the formation of ZnO nanorods. Other authors observed similar peaks below 400 nm (350−370 nm) due to the electronic transition from the valence band to the conduction band. The literature study indicates that the bulk ZnO particles absorb around 380 nm, while the absorption of ZnO nanoparticles is blue-shifted to different wavelengths from 375 to 350.[42] The prepared ZnO nanorods show a redshift in the absorption band, which may be attributed to the aggregation of the nanorods, resulting in larger nanostructures and/or the presence of the zincate ions like $Zn(OH)_2$, $[Zn(OH)_3]^-$, $[Zn(OH)_4]^{2-}$, and traces of TEA. Such redshifts of the characteristic absorptions of the Zn−O bond in ZnO are also reported by other authors. Koutu et al.[43] observed a reduction in size of the as-prepared ZnO nanostructures as the NaOH concentration increased, which may be due to the fast nucleation during the synthesis process. But literature survey shows that the size of the nanostructure increases as the NaOH concentration increases. According to the Ostwald ripening theory,[44,45] during synthesis, tiny crystallites nucleate first and then agglomerate into larger crystallites due to the energy difference between large and smaller particles of higher solubility based on the Gibbs−

Thomson law.[46] This increases the number of energy states of the material substantially, thereby decreasing the energy gap (the band gap) between the highest occupied valence band and the lowest occupied conduction band, leading to a redshift. C-doped ZnO-NPs, prepared by irradiating the Zn granules with CO_2 microwave plasma from a torch, were reported to show a significant redshift in the absorption edge to lower energy due to band gap narrowing. The authors suggested that the carbon species are incorporated into the O site of ZnO in the process of synthesis.[47]

3.1.3. FT-IR Spectrum of ZnO Nanorods. Figure 1b shows the FT-IR spectrum of ZnO nanorod in the range of 500−4000 cm^{-1}. The broad absorption around 3414 cm^{-1} and that around 1140 cm^{-1} are due to the O−H stretching and C−O/C−N stretching vibrations, respectively, of the triethanolamine, which is adsorbed on the ZnO and the residual $Zn(OH)_2$, respectively. The absorption band around 618 cm^{-1} is identified as the characteristic band of the ZnO nanorod.

Generally, characteristic absorptions of the ZnO nanoparticles appear below 600 cm^{-1} like any other metal oxide.[48,49] The absorption bands due to the Zn−O bond vibrations in ZnO nanoparticles have been reported in the literature at 417.5,[50] 477,[38] 480,[40] 482, 595,[51] and 500 cm^{-1},[52] and the difference in absorptions is attributed to difference in particle sizes. Soni et al.[53] attributed the band observed around 520 cm^{-1} to the wurtzite hexagonal shape of pure ZnO nanorod.

Andrés-Vergés et al.[54,55] discussed the dependence of the IR spectrum of ZnO particles on various geometrical shapes and suggested that the origin of IR bands at 475 and 494 cm^{-1} is due to the $ZnO/Zn(OH)_2^-$ citrate complex on the surface and bulk of the ZnO in the solid state. On calcination at 300 °C, bands at 440 and 529 cm^{-1} appear.[48] The FT-IR spectrum of the ZnO nanoparticles synthesized by a novel green route using natural biodegradable polymer showed a broad band around 457 cm^{-1} and a shoulder around 545 cm^{-1} corresponding to ZnO nanoparticles according to the authors.[56] Singh et al.[57] reported that the characteristic Zn−O vibration appears at 782 cm^{-1} for the ZnO nanoparticles prepared using zinc acetate and Coriandrum sativum leaf extract. The band at 533 cm^{-1} was reported to be the characteristic absorption of Zn−O bond for ZnO nanoparticle with 77.56% of zinc and 22.44% of oxygen (from EDAX studies).[58] The absorption at 620.93 cm^{-1} was reported to correspond to the Zn−O bond deformation vibration for the ZnO nanoparticles prepared using zinc sulfate heptahydrate as the precursor, hydrazine hydrate as the surfactant, and PVP as the stabilizer.[59]

The absorption at 618 cm^{-1} for the ZnO nanorods prepared in our present study may be due to the difference in particle size and geometry or to the presence of traces of TEA and the $Zn(OH)_2$ as indicated by the EDAX data (zinc—48% and oxygen—52%).

3.1.4. Powder XRD Pattern of ZnO Nanorod. Figure 1c shows the powder XRD pattern of the ZnO nanorod synthesized by the sol−gel method. This XRD pattern shows distinct peaks at 31.7, 34.38, 36.19, 47.48, 62.67, 62.84, 67.87, 69.07, and 72.61° corresponding to different diffraction planes (100), (002), (101), (102), (110), (103), (112), (201), and (004) of the ZnO nanorod. The presence of these peaks in the XRD pattern confirms the shape of ZnO as short nanorods as reported elsewhere.[60] All of the peaks in the powder XRD pattern of ZnO nanorods are very sharp, showing that the

prepared ZnO nanorods are highly crystalline. The powder XRD pattern of ZnO nanorods is in good agreement with that reported in the literature (ICCD No. 01-080-0075).

3.1.5. TGA/DTG of ZnO Nanorods. TGA/DTG curves of the as-synthesized ZnO nanorod samples prepared by the sol–gel method are given in Figure 1d,e. These curves reveal that the weight loss for ZnO stopped at 480 °C. In the DTG curves of the samples, three different kinds of peaks were observed. The first one below 100 °C is due to the removal of moisture. The second stage degradation with a weight loss of 0.4%, observed around 280 °C, is mainly due to the loss/decomposition of traces of triethanolamine (adhering to ZnO nanorods), used in the preparation of ZnO as a stabilizer. The third-stage degradation indicated by the peak around 480 °C was assigned to the conversion of traces of $Zn(OH)_2$ (present along with the ZnO nanorods as indicated by the FT-IR and EDAX analyses) to ZnO. The ZnO nanorods are found to be stable beyond this temperature as no more weight loss was observed beyond 480 °C. Similar observations were found in the literature.[61] The degradation peak around 430 °C is reported to be due to the conversion of $Zn(OH)_2$ into ZnO, and beyond 434 °C, no weight losses were observed in the TGA curve of ZnO.[61] But Kołodziejczak-Radzimska et al. reported up to 20% weight loss in the TGA of ZnO particles synthesized by the emulsion precipitation method.[62]

3.1.6. FE-SEM Image of ZnO Nanorods. The nanoparticles of ZnO prepared by different methods and using different precursors have different morphologies like spherical particles, flower-like morphology, flake-like morphology, rodlike morphology, etc. The FE-SEM image of the prepared ZnO, obtained with a magnification of 5000× on a glass substrate is shown in Figure 1f, which indicates a rodlike morphology with an average diameter of 350 nm and an average length of 700 nm (1 μm = 1000 nm). Such high diameters indicate agglomeration of the particles, and hence further analysis using TEM was carried out. The particle size of about 85 nm was reported for the ZnO nanopowder with rodlike morphology prepared using zinc acetate dihydrate, sodium hydroxide, and ethanol by the sol–gel method. Hasnidawani et al.[63] observed that ZnO can be formed in different morphologies based on the type of precursor that has been used, viz., zinc acetate nano-rodlike structure, zinc chloride and sulfate nanoprism structure, and zinc nitrate prism flower-shaped structure. Handore et al.[56] reported uniform and multifaceted morphology. Haque et al. reported well-defined hexagonal rodlike structure for the ZnO prepared from zinc acetate, and TEA.[40] Osman et al. reported different morphologies of platelets, flaky particles, nanotubes, spherical, and nanorods.[64] Ban et al. reported that on increasing the base tetramethyl ammonium hydroxide/Zn ratio, the shape of the resulting ZnO crystals changed from a short asymmetric column with a hexagonal flat edge and a rounded one, through a rocket-like shape formed by intergrowth, to a hexagonal rod.[41]

3.1.7. FE-SEM-EDAX Analysis of ZnO Nanorod. Figure 1g shows the FE-SEM-EDAX image and spectrum of the prepared ZnO nanorod sample; the EDX spectra clearly reflect the presence of zinc (48%) and oxygen (52%). But the actual compositions of zinc and oxygen in pure zinc oxide are 80.2 and 19.8%, respectively. The additional peak in the EDAX spectrum (Figure 1h) and the stoichiometry of zinc and oxygen differing from that of the theoretical value may be due to the presence of traces of TEA adsorbed on the ZnO

nanorod or the traces of $Zn(OH)_2$ in the sample. Analysis of the literature reveals that a few authors reported the zinc–oxygen compositions almost close to the stoichiometry in the molecule,[49] while others reported varying compositions. Hasnidawani et al.[63] reported 55.38% zinc content and 44.62% oxygen content for ZnO nanopowder prepared by sol–gel method using zinc acetate dihydrate, sodium hydroxide, and ethanol. Shamhari et al. reported, based on EDX studies, that the ZnO nanoparticles prepared by solvothermal process using zinc acetate dihydrate, absolute ethanol, and potassium hydroxide have 76.3% Zn and 23.7% O.[65] Soni et al. reported the weight percentage ratio of zinc to oxygen as 79.50:20.50 using EDAX analysis, which is almost consistent with stoichiometric ZnO.[53]

3.1.8. HR-TEM Image of ZnO Nanorods. TEM analysis was employed to further investigate and confirm the morphology and size of the prepared ZnO nanostructures. Figure 1i shows the HR-TEM image of ZnO nanorods. The statistical analysis indicates that the average nanorod diameter and length are 20 and 40 nm, respectively. The image reveals a short rodlike morphology for ZnO nanorods. Soni et al. reported diameters and lengths ranging from 25 to 30 nm and from ~0.3 to 3 μm, respectively, for the ZnO nanorods synthesized using zinc acetate, methanol, and sodium hydroxide.[53]

3.2. FT-IR Spectroscopy of Banana Fiber. Figure 2 shows the FT-IR spectra of the unmodified and chemically
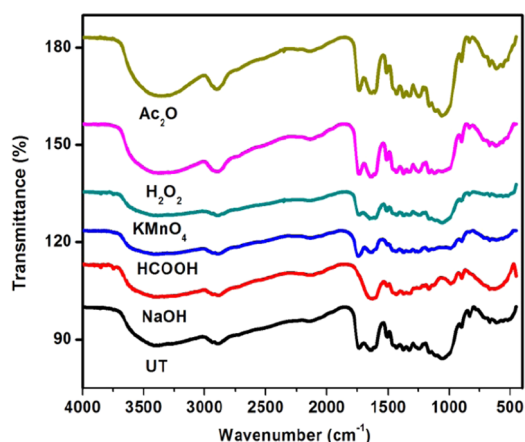
Figure 2. FT-IR spectra of untreated and chemically treated banana fibers.

modified banana fibers. The FT-IR spectrum of the unmodified banana fiber consists of absorption bands in the region of 800–3400 cm^{-1} characteristic of the stretching vibrations of O–H, C=O, C=C, and CH_2 groups.[66] All of the characteristic bands shifted to lower wavenumbers after treatment with 5% NaOH, and the intensity of the absorption bands due to the –OH is reduced in comparison to that of the untreated banana fiber. Treatment with other reagents, viz., HCOOH and $KMnO_4$ also led to a similar reduction in the intensity of the OH bands. But with the Ac_2O and H_2O_2 treatments, an increase in the intensity of the OH bands was observed. Another weak band around 2916 cm^{-1} assigned to the C–H stretching vibrations of the aliphatic C–H bond also shows similar types of changes on treatment with the respective reagents due to the removal of xylan, a type of hemicellulose.[67,68] Figure 2 clearly shows that the band at 1736 cm^{-1} due to the C=O groups present in lignin and
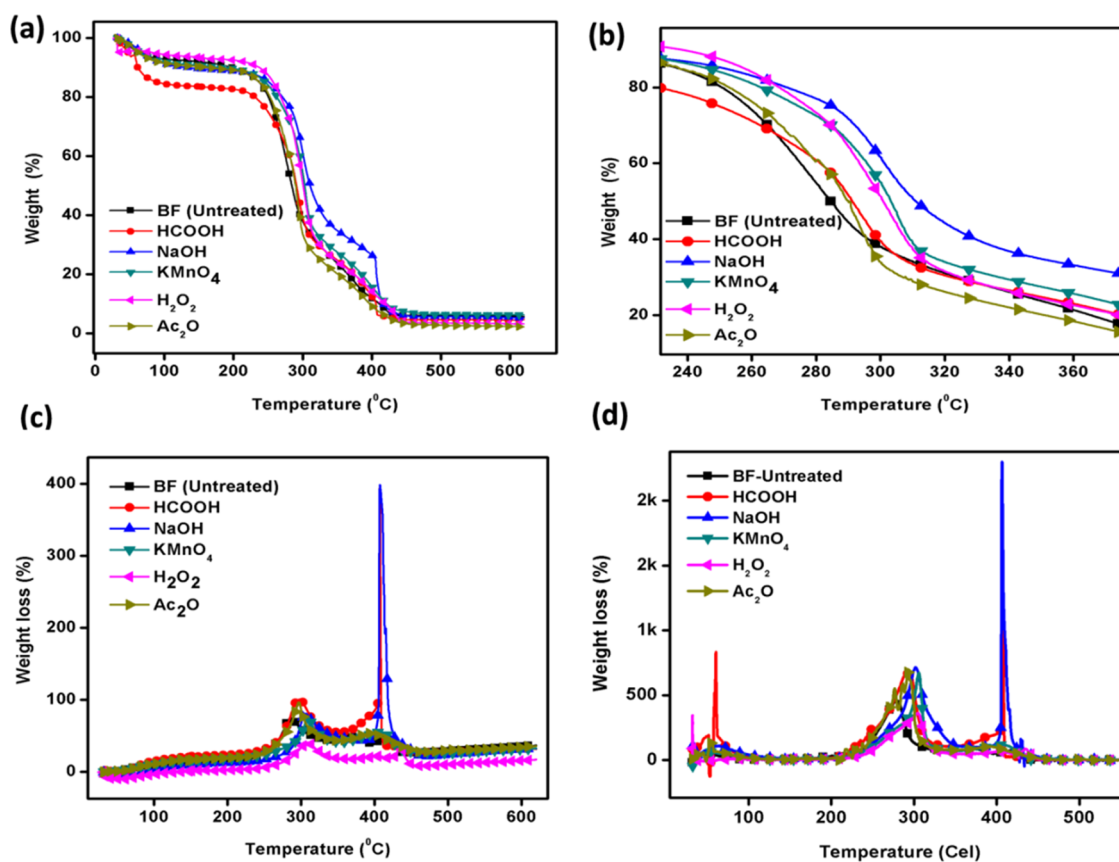
Figure 3. (a) TGA curves, (b) expanded TGA curves, (c) DTG curves, and (d) expanded DTG curves of untreated and chemically treated banana fibers.

hemicelluloses completely disappeared after 5% NaOH treatment. After KMnO$_4$ treatment, the intensity of the same band decreased significantly, while with H$_2$O$_2$ treatment, only a small decrease was observed. With Ac$_2$O and H$_2$O$_2$ treatments, the intensity of the bands due to >C=O stretching vibrations was found to be enhanced. This is due to the removal of the constituents of hemicelluloses and lignin on the banana fiber. The bands around 1654 and 1251 cm^{-1} are assigned to the >C=O (acetyl) group present in lignin.[68,69] The intensities of these bands were also decreased on chemical treatments. This is because of the partial removal of lignin on the fiber surface. The next band 1434 cm^{-1} can be assigned to the aromatic skeletal vibrations of lignin combined with C−H in-plane deformation of the CH$_2$ groups of cellulose. Another broad band at 1021 cm^{-1} is due to the C4−OH of the glucose residue in the cellulosic part of the raw banana fiber. The intensity of this band also undergoes reduction on chemical treatments. The NaOH, HCOOH, and KMnO$_4$ treatments bring about better removal of the constituents of the fiber, namely, hemicellulose and lignin compared with H$_2$O$_2$ and Ac$_2$O treatments. Particularly, among the various chemical treatments carried out in the present study, alkali treatment seems to be better for banana fiber as it removes lignin and other impurities effectively.

3.3. Thermal Analysis of Untreated and Chemically Treated Banana Fibers. Figure 3a−d shows the TGA/DTA curves and the expanded TGA/DTA curves of untreated and chemically treated banana fibers. All of the natural fibers consist of several constituents such as cellulose, hemicellulose or xylan, lignin, oily waxes, moisture content, and other

impurities in varying quantities. Thermograms of all of the natural fibers show almost similar trends with very slight differences; they decompose in three main stages as noted by other authors reported in the literature.[70−73] The first-, second-, and final-stage decompositions for the natural fibers, in general, are reportedly found around 30−150, 150−350, and 275−380 °C, due to the evaporation of moisture, decomposition of hemicellulose or xylan, and cellulose degradation, respectively. In the present study, the weight loss found in the TGA curve below 100 °C is assigned to the evaporation of moisture for the untreated and treated banana fibers (Figure 3a,b). Figure 3c shows that the DTG curves of the untreated banana fiber consist of two distinct peaks. The first weight loss noted at 285−375 °C is attributed to the hemicelluloses and the next peak noted between 375 and 416 °C is assigned to cellulose degradation of untreated banana fiber. Table 1 shows the peak decomposition temperatures obtained from the DTG curves of untreated and chemically (such as NaOH, HCOOH, Ac$_2$O, H$_2$O$_2$, and KMnO$_4$) treated banana fibers. The results

Table 1. Peak Temperatures Obtained from the DTG Curves of Untreated and Chemically Treated Banana Fiber

S. No.	sample code	peak I (°C)	peak II (°C)	peak III (°C)
1	BF-UT	285	375	416
2	BF-HCOOH	297	409	431
3	BF-NaOH	307	406	447
4	BF-KMnO$_4$	310	409	465
5	BF-H$_2$O$_2$	308	409	435
6	BF-AC$_2$O	298	394	501
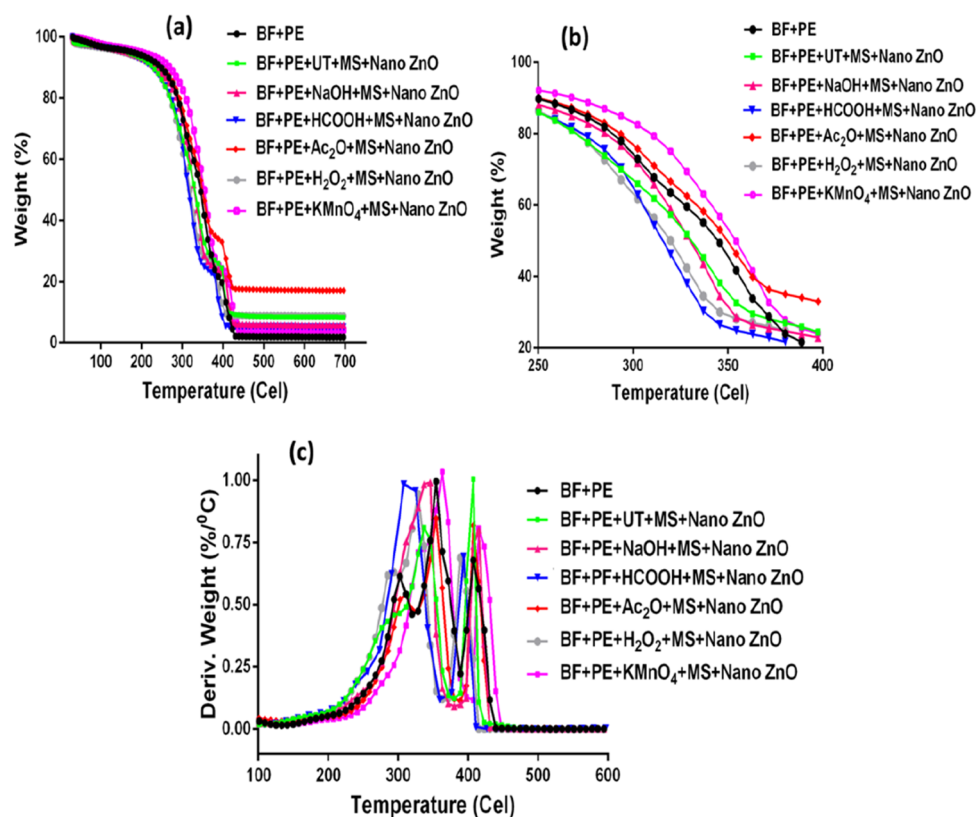
Figure 4. (a) TGA curve, (b) expanded TGA curve, and (c) DTG curve of unmodified and chemically modified BF fiber/PE/MS/ZnO hybrid nanobiocomposites.

show that the thermal degradation temperature increases in the order of UT < HCOOH < H_2O_2 < NaOH < $KMnO_4$ < Ac_2O. However, the thermal stability of Ac_2O-treated fiber is found to be higher than that of the untreated fiber and other chemically treated banana fibers.

3.4. Thermal Stability of Untreated and Chemically Treated BF Fiber/PE/Molecular Sieves Filled ZnO Nanorod Hybrid Nanobiocomposites. The TGA, expanded TGA, and DTG thermograms of the untreated and chemically treated short BF fiber-reinforced unsaturated polyester biocomposite and the nanobiocomposites with molecular sieves + ZnO nanorod are given in Figure 4a−c. Peak temperatures obtained from the DTG curves are given in Table 2. The increasing temperature gradually increased the weight loss of all of the biocomposites and nanobiocomposites. The weight loss below 100 °C is associated with the evaporation of water from the composites (Figure 4a). Two major degradation peaks are observed in the DTG curve

(Figure 4c). The first major weight loss at around 350 °C (starting from 250 °C) is related to the degradation of the cellulose fiber. The second major weight loss around 450 °C (starting from 350 °C) is related to the degradation of the PE matrix. The BF + PE biocomposites were found to have better degradation temperature compared with BF + PE + UT + MS + nano ZnO nanocomposites.

$KMnO_4$-treated BF + PE + MS + nano ZnO nanorod-filled nanobiocomposites show the highest thermal stability among all of the treated/untreated BF-reinforced nanobiocomposites and biocomposites.

The decreasing order of the first decomposition temperature corresponding to the BF fibers in the nanobiocomposites/ biocomposites for the various chemical treatments is $KMnO_4$ (367.21 °C) > Ac_2O(356.13 °C) > BF + PE (354.18 °C) > NaOH (343.10 °C) > BF + PE + UT + MS + nano ZnO (340.7 °C) > H_2O_2 (330.06 °C) > HCOOH (307.70 °C).

In a previous report,[73b] the authors reported that the composite samples reinforced with alkali-, $KMnO_4$-, and formic acid-treated natural fibers have a higher degradation temperature in comparison to the untreated composites. On the other hand, for benzoylation, acetylation, and silane treatment, the hydrophilicity of the fiber surface decreased and the void content increased. This leads to weak chemical bonding at the fiber/matrix interface. In our study, an increase in the degradation temperature was observed for the $KMnO_4$- and Ac_2O-treated BF + PE + MS + nano ZnO filled nanobiocomposites in comparison to the untreated nanobiocomposites. NaOH, H_2O_2, and HCOOH-treated BF + PE + MS + nano ZnO nanobiocomposites were found to a have lower degradation temperature compared with untreated nanobiocomposites.

Table 2. Thermal Analysis Data of Unmodified/Chemically Modified BF Fiber/PE/Molecular Sieves Filled ZnO Nanorod Hybrid Nanobiocomposite

sample	peak I (°C)	peak II (°C)
BF + PE	354.2	406.5
BF + PE + UT + MS + nano ZnO	340.6	402.6
BF + PE + NaOH + MS + nano ZnO	343.1	410.2
BF + PF + HCOOH + MS + nano ZnO	307.7	391.5
BF + PE + Ac_2O + MS + nano ZnO	356.1	408.3
BF + PE + H_2O_2 + MS + nano ZnO	330.1	385.9
BF + PE + $KMnO_4$ + MS + nano ZnO	367.2	417.6

3.5. Effect of Various Chemical Treatments and ZnO Nanorod on the Mechanical Properties, and Water Absorption of Short BF/PE/Molecular Sieves + ZnO Nanorod Hybrid Nanobiocomposites. *3.5.1. Tensile Strength.* The tensile strengths of randomly oriented banana fiber-reinforced unsaturated polyester/molecular sieves/ZnO nanorod-filled hybrid nanobiocomposites (BF/PE/MS + ZnO nanorod) and BF/PE/MS biocomposites with and without chemical treatment of the banana fibers are given in Table 3 and Figure 6a. The chemical treatment of the banana fiber with all of the chemicals (NaOH, HCOOH, Ac_2O, H_2O_2, $KMnO_4$) leads to a decrease in the tensile strength of the BF/PE/MS biocomposites, although only a very moderate decrease was observed for H_2O_2 and $KMnO_4$ treatments. This is in contrast to the general observation of enhanced tensile properties on chemical treatment of the natural fibers. The increase is attributed to the removal of waxy materials, hemicellulose, lignin, etc. But a few other authors have reported a decrease in the tensile strength of the biocomposites on chemical treatment of the natural fibers.[74−76] The decrease in tensile strength may be due to the excess delignification of natural fiber at higher alkali concentration resulting in a weaker or damaged fiber or the degradation of the fibrous material in addition to lignin. $KMnO_4$ treatment is reported to enhance the tensile strength of abaca fibers at low concentrations and shorter treatment times. At high concentrations and longer treatment times, a decrease in tensile strength was observed.[77] A study on the effect of NaOH concentration (0.5, 1, 2, 4, and 10%) for treating sisal fiber reveals that the maximum tensile strength was obtained for the sisal/polyester composites from the 4% NaOH treatment and higher tensile strength for 5% NaOH treatment than for 10% NaOH treatment.[78]

The addition of 2% of ZnO nanorods increased the tensile strength of all of the chemically treated BF/PE/MS biocomposites. The addition of ZnO nanorod to the BF + PE +UT + MS biocomposite does not bring about such an increase (Table 3) The untreated bionanocomposite BF + PE + MS+nano ZnO has a lower tensile strength of 18.0 MPa The tensile strength decreased (from 26.0 to 18.6 MPa) in the following order for the various chemically treated banana fiber-reinforced bionanocomposites, though the differences are very small BF + PE + NaOH + MS+ nano ZnO > BF + PE + HCOOH + MS + nano ZnO > BF + PE + $KMnO_4$ + MS + nano ZnO > BF + PE + H_2O_2 + MS + nano ZnO > BF + PE + Ac_2O + MS + nano ZnO. Only a slight decrease was observed for the NaOH, HCOOH, and $KMnO_4$ treatments, while significant decreases were noticed for H_2O_2 and Ac_2O treatments, although FT-IR (Figure 2) and SEM images (Figure 5) indicate the removal of lignin and hemicelluloses.

In a previous study, sisal/banana hybrid biocomposites were found to show improvement in the tensile properties with the addition of Al_2O_3 nanopowder. The addition of 3 wt % of nanopowder enhanced the tensile properties from 41.1 to 55.75 MPa. The incorporation of nanofiller provides more interfacial interaction between filler and resin, resulting in wettability enhancement.[79] Other authors reported that the coir/wood/MMT/PP hybrid nanocomposite displayed better tensile properties than coir/wood/PP, wood/PP, and coir/PP composites because of more effective stress transfer between the fibers in the presence of MMT. The nanoclay enhanced interfacial interaction and adhesion between the fiber and the polymer matrix, thus improving the mechanical properties of the composites.[80] Hybridization involving the combination of

Table 3. Mechanical Properties and Water Absorption of Short Banana Fiber/PE/MS and Banana Fiber/PE/MS/ZnO Nanorod Hybrid Nanocomposites without/with Different Chemical Treatment

S. No.	name of the sample	tensile strength [MPa] without nano mean ± SD	tensile strength [MPa] with nano mean ± SD	compressive strength [MPa] with nano mean ± SD	compressive strength [MPa] without nano mean ± SD	flexural strength [MPa] with nano mean ± SD	flexural strength [MPa] with nano mean ± SD	Izod impact value [J m⁻¹] without nano mean ± SD	Izod impact value [J m⁻¹] without nano mean ± SD	% water absorption test without nano mean ± SD	% water absorption test with nano mean ± SD
1	BF + PE (UT)	18.7 ± 2.664	18.0 ± 4.045	25.9 ± 2.501	24.0 ± 1.799	51.6 ± 6.404	49.0 ± 8.656	0.36 ± 0.020	0.31 ± 0.010	25.2 ± 0.929	24.3 ± 3.306
2	BF + PE + MS + NaOH	14.6 ± 3.502	26.0 ± 1.825	15.4 ± 3.168	48.5 ± 2.127	62.9 ± 5.275	49.1 ± 2.545	0.40 ± 0.100	0.83 ± 0.247	17.7 ± 2.452	18.8 ± 6.200
3	BF + PE + MS + HCOOH	13.1 ± 2.085	25.0 ± 9.988	6.9 ± 1.473	41.6 ± 2.573	43.7 ± 11.761	55.7 ± 9.280	0.50 ± 0.100	1.45 ± 0.328	39.0 ± 15.694	20.9 ± 1.873
4	BF + PE + MS + Ac₂O	18.2 ± 1.385	18.6 ± 4.629	7.9 ± 2.241	34.6 ± 1.972	29.6 ± 12.608	59.4 ± 17.597	0.62 ± 0.247	0.82 ± 0.548	27.2 ± 6.809	21.6 ± 6.296
5	BF + PE + MS + H₂O₂	13.5 ± 1.752	24.7 ± 0.814	9.9 ± 2.268	37.0 ± 1.809	69.0 ± 9.410	79.0 ± 6.034	0.43 ± 0.153	0.67 ± 0.144	33.9 ± 4.025	14.5 ± 3.625
6	BF + PE + MS + KMnO₄	17.6 ± 5.430	24.7 ± 4.510	14.5 ± 0.426	39.4 ± 3.534	42.2 ± 5.537	67.4 ± 5.308	0.40 ± 0.100	0.60 ± 0.132	49.6 ± 7.112	15.5 ± 1.970
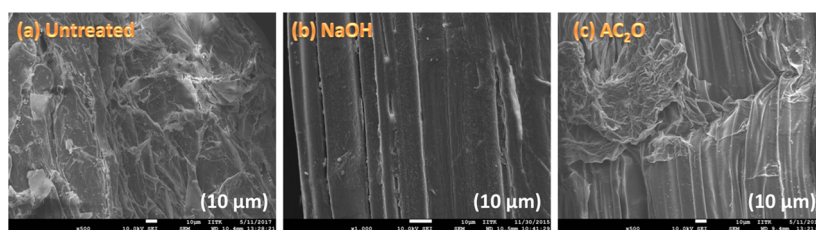
Figure 5. SEM images of (a) untreated, (b) NaOH-treated, and (c) Ac$_2$O-treated banana fibers.
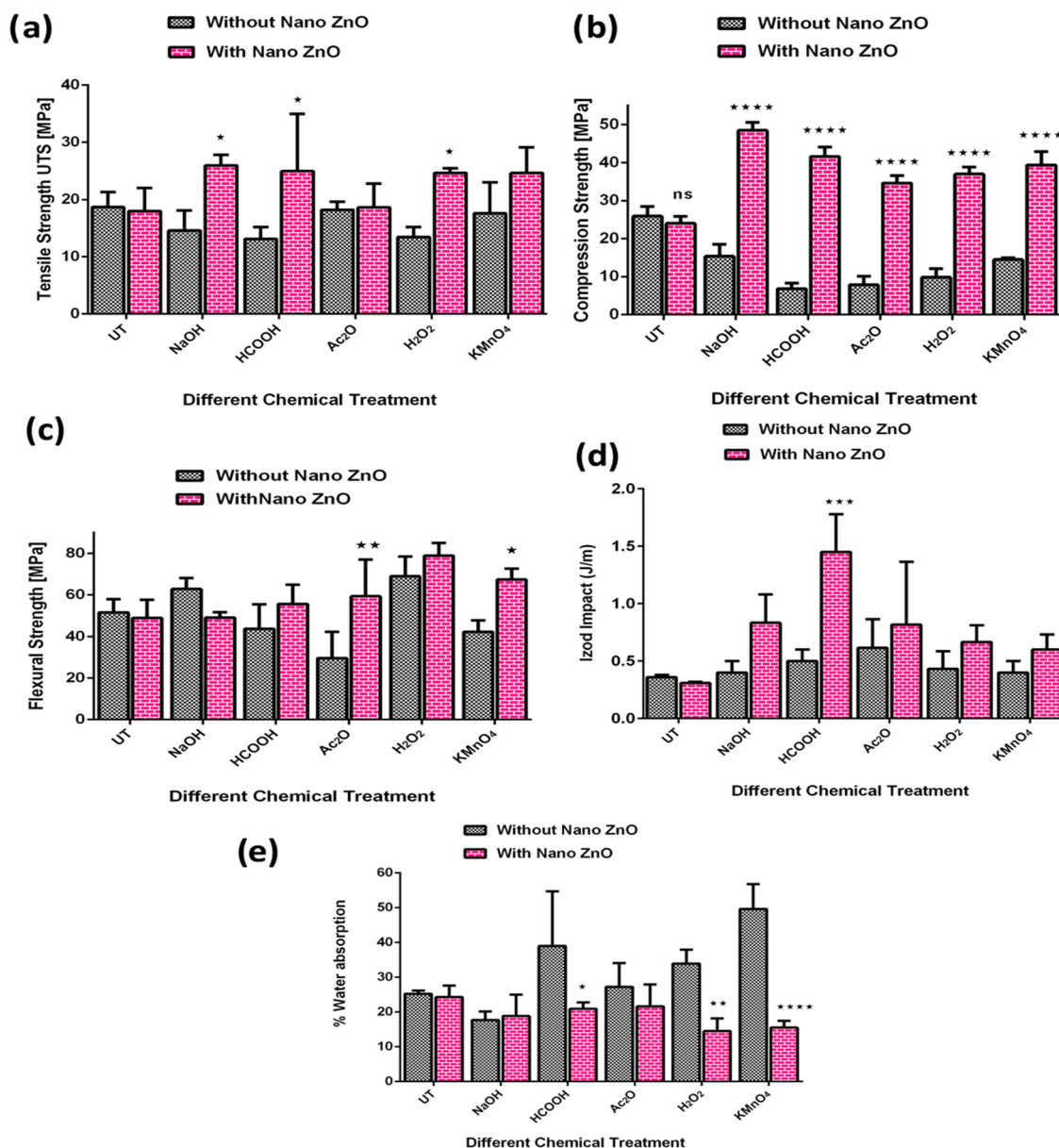
Figure 6. Effect of different chemical treatments on the (a) tensile strength, (b) compressive strength, (c) flexural strength, (d) impact strength, and (e) % water absorption of short BF/PE/MS biocomposites and short BF /PE/MS/ZnO hybrid nanobiocomposites.

nanofiller and natural fiber in the polymer matrix results in increased mechanical properties.[81]

3.5.2. Compressive Strength. The compressive strengths of the hybrid biocomposites BF + PE + MS and hybrid nanobiocomposites BF/PE/MS + ZnO with untreated and chemically treated short randomly oriented banana fiber are given in Figure 6b and Table 3. The compressive strengths of all of the biocomposites and nanobiocomposites prepared in

the present study were found to be significantly higher than the tensile strength. Such observations were made by other authors for the woven kenaf fiber-reinforced unsaturated polyester biocomposites.[82] A significant decrease in the compressive strength of the BF + PE + MS biocomposites was noticed when chemically treated banana fibers were used instead of untreated fibers. Similar observations were reported in the literature.[83] NaOH-treated banana fiber/eco-polyester compo-
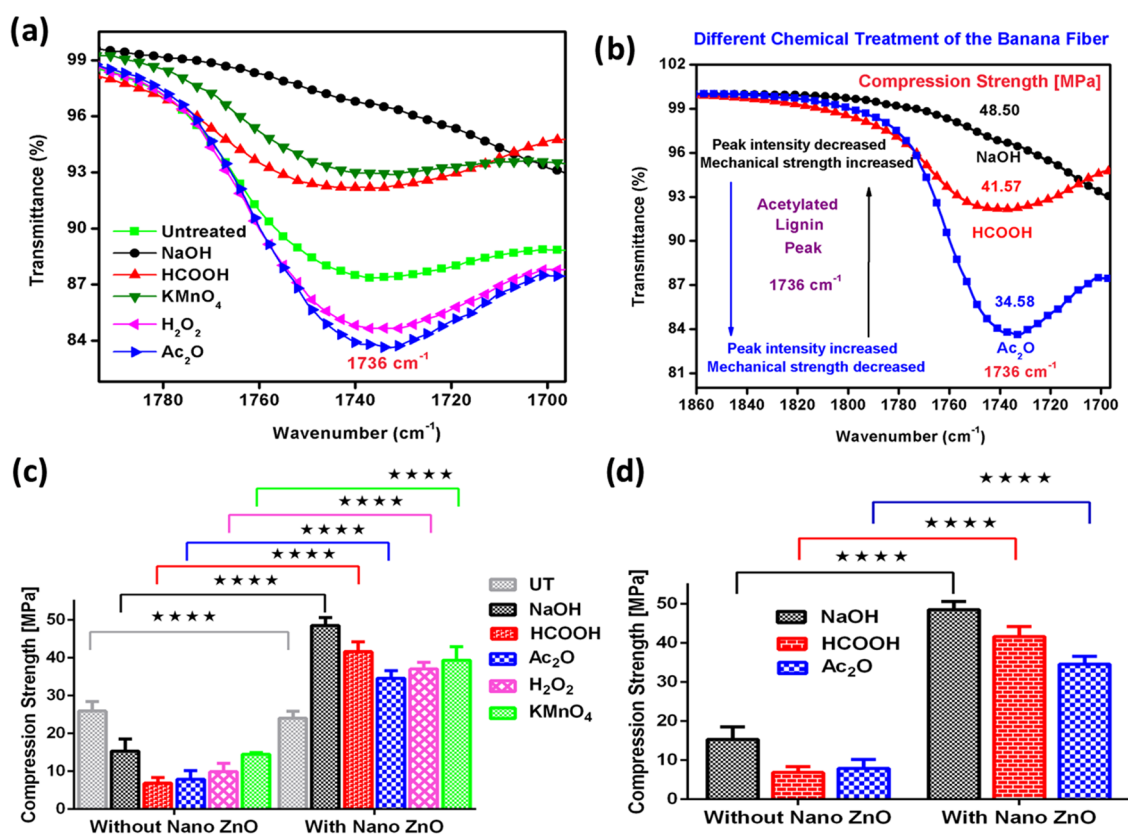
Figure 7. (a) FT-IR spectra of NaOH-, HCOOH-, H_2O_2-, Ac_2O-, and $KMnO_4$-treated banana fibers. (b) Comparison of the compressive strengths of NaOH-, HCOOH-, and Ac_2O-treated BF + PE + MS + ZnO hybrid nanobiocomposites with the intensity of the absorption band at 1736 cm^{-1} in the respective FT-IR spectra. (c) Comparison of the effect of ZnO nanorods on the compressive strength of different chemically treated BF + PE + MS + ZnO hybrid nanobiocomposites and BF + PE + MS hybrid biocomposites (****P < 0.0001). (d) Comparison of the effect of ZnO nanorods on the compressive strengths of NaOH-, HCOOH-, and Ac_2O-treated BF + PE + MS + ZnO hybrid nanobiocomposites and BF + PE + MS hybrid biocomposites (****P < 0.0001) P values are with respect to the control (biocomposites with and without ZnO nanorods).

sites have lower compressive strength (84.70 ± 5.12 MPa) than the untreated banana fiber/eco-polyester composites (122.88 ± 2.54 MPa), although a reverse trend was reported for the epoxy-based composites.[83] Previous work revealed that chemical treatments increase surface roughness and decrease surface polarity.[84] NaOH cleans the surface of the fiber by removing impurities, waxes, and part of the lignin acts as a cementing substance that holds the fibrils together. Partial removal of lignin causes some debonding of the fibrils, which leads to exposure or protruding of some of them. Such protrusion will produce mechanical bonding of the fibers and consequently improve fiber–matrix interaction and hence enhanced strength.[48,49] But the BF + PE + MS + ZnO hybrid bionanocomposites show a much higher compressive strength only with chemically treated fibers (especially NaOH) (Table 3). BF + PE + MS + ZnO hybrid nanobiocomposites made with untreated fibers have compressive strength comparable to that of the respective biocomposite (Table 3). The chemical treatment of the fiber and the addition of nanofiller together give very high compressive strength to the BF + PE + MS biocomposites. In the BF/PE/MS + ZnO nanobiocomposite, the addition of 2% ZnO nanorod to the polyester resin matrix, which already contains banana fiber and molecular sieves, moderately increased the compatibility between fiber/matrix and MS/matrix, thereby increasing the compressive strength. Similar observations were made by Mohan et al. They reported that nanoclay-infused banana fiber resulted in a 43% increase in the ultimate compressive strength of the banana fiber-

reinforced epoxy composite cylinders, compared to the composite cylinders without nanoclay.[85]

The intensity of the band at 1736 cm^{-1} in the FT-IR spectrum (Figure 7a,b) due to the ester and carbonyl group of lignin present in the banana fiber was found to decrease on treatment with HCOOH; with Ac_2O treatment, this band has a very high intensity, indicating that the removal is not very efficient; with NaOH treatment, this band has almost vanished, showing that the lignin is almost completely removed. Accordingly, the compressive strength of the BF/PE/MS + NaOH + ZnO nanobiocomposite is the highest; that of the BF/PE/MS + HCOOH + ZnO nanobiocomposite is moderate; and that of the BF/PE/MS + Ac_2O + ZnO nanobiocomposite is the lowest.

3.5.3. Flexural Strength. The flexural strengths of BF/PE/MS + nano ZnO in the BF/PE/MS hybrid biocomposites and BF/PE/MS + ZnO hybrid nanobiocomposites are given in Figure 6c and Table 3. The H_2O_2- and NaOH-treated BF/PE/MS hybrid biocomposites showed improved flexural strength (69.0 and 62.9 MPa, respectively) compared to the untreated BF/PE/MS hybrid biocomposites (51.6 MPa), while the $KMnO_4$, Ac_2O, and HCOOH treatments decreased the flexural strength. Alfafiber-reinforced polyester composites show improved flexural strength after treatment with NaOH.[86] All of the chemically treated BF/PE/MS + ZnO hybrid nanobiocomposites have improved flexural properties after adding ZnO nanorods except NaOH-treated BF/PE/MS + ZnO hybrid nanobiocomposites. The H_2O_2 and $KMnO_4$ treatments

and ZnO together give the highest flexural strength. The untreated BF/PE/MS + ZnO hybrid nanobiocomposite was found to have lower flexural strength than the corresponding biocomposite.

The added ZnO nanorods should have enhanced the interfacial bonding between the banana fiber and the polyester matrix. Also, the ZnO nanorods having the residual hydroxide groups is strongly bonded to the fibers and the nonpolar parts of the ZnO are associated with the polyester matrix.

Similarly, the $KMnO_4$-, Ac_2O-, and HCOOH-treated hybrid nanobiocomposites were found to have moderately high flexural strength compared with the corresponding biocomposites. Goriparthi et al.[87] reported that the flexural strength of alkali-, peroxide-, permanganate-, and silane-treated jute fiber-reinforced polylactic acid composites are higher than that of the untreated fiber composites.

3.5.4. Izod Impact Properties. Figure 6d and Table 3 show the Izod impact properties of untreated and chemically treated short BF/PE/MS biocomposites and chemically treated BF/PE/MS + ZnO hybrid nanobiocomposites. The impact strength of the untreated BF/PE/MS biocomposite was increased considerably by all of the chemical treatments used in the present study. The addition of ZnO nanorods further enhanced the impact strength (Table 3). Pretreatment of the banana fiber and the addition of ZnO nanorod together gave the highest flexural strength of 1.45 J m^{-1}. The addition of 1% of MMT into the kenaf fiber-polyester system showed improved impact properties. Further addition led to agglomeration of MMT particles, causing a decrease in impact strength.[88] Literature study reveals that addition of biosynthesized alumina nanoparticles to hybrid banana/coir, sisal/coir, and sisal/banana biocomposites enhanced the impact strength by 9.65, 12.64, and 7.12%, respectively.[89] The addition of baggase ash particles to hybrid sisal/flax and sisal/kenaf biocomposites enhanced the impact strength.[90]

3.5.5. Water Absorption Properties. The water absorption properties of untreated/chemically treated short BF/PE/MS biocomposites and BF/PE/MS + ZnO hybrid nanobiocomposites are illustrated in Figure 6e and Table 3. Banana fiber, a natural fiber, is strongly hydrophilic with many hydroxyl groups (−OH) and absorbs moisture heavily due to the formation of hydrogen bonds with water molecules.[91] Alkali treatment leads to an improvement in interfacial bonding, hence promoting resin/fiber interpenetration at the interface, by providing additional sites for mechanical interlocking.[92] The NaOH-treated woven fan palm fiber-reinforced (WFP) unsaturated polyester composites have a lower water absorption percentage compared to untreated WFP composites.[93] However, our results reveal that all of the chemically treated BF/PE/MS biocomposites (except NaOH treatment) absorb much larger quantities of water than the untreated BF/PE/MS biocomposites. This may be because of the presence of molecular sieves, which have lot of voids and are known to absorb water and other solvent molecules extensively.

All of the chemically treated short BF/PE/MS + ZnO hybrid nanobiocomposites have lower moisture absorption than the respective BF/PE/MS biocomposites. This observation suggests that the addition of ZnO nanorods interfered with the absorption of water. Similar results of reduced water absorption by the addition of nanomaterials were reported in the literature.

The H_2O_2-treated hybrid nanobiocomposites show the highest resistance to water absorption among all of the nanobiocomposites prepared in this work. In the previous results, NaOH-treated jute fiber/unsaturated polyester composites were reported to show only 2.5% of water absorption after immersion in normal water for 250 h. This illustrates the effectiveness of alkaline treatment of jute fiber in the reduction of water absorption. A further decrease in water absorption was noticed on the incorporation of Al_2O_3/ZrO_2. Better compatibility between hydrophobic metal oxides and hydrophobic polyester might have attributed to the reduction of water absorption.[92] Reduction in the hydrophilicity of the composites is advantageous for many applications. The water mass uptake of sisal fiber-reinforced composites based on epoxy polymer and three levels of nanoclay (1, 3, and 5 wt %) were studied by Mohan and Kanny et al. The result showed a dramatic decrease in water mass uptake of nanoclay-filled composites by increasing the nanoclay content. Hybridization involving the combination of nanofiller and natural fiber in the polymer matrix results in the reduction of water absorption properties.[30,81] Generally, the composite materials with low water absorption must be most suitable for many automotive applications such as car wheel shield, panels, etc.

4. CONCLUSIONS

Untreated and chemically treated short BF/PE/MS biocomposites and chemically treated BF/PE/MS + ZnO hybrid nanobiocomposites were made using the ZnO nanorods prepared in our laboratory. $KMnO_4$ treatment increased the thermal stability, while the NaOH, H_2O_2, and HCOOH treatments decreased the thermal stability of nanobiocomposites. Pretreatment of the banana fibers with NaOH, HCOOH, H_2O_2, Ac_2O, and $KMnO_4$ led to a significant decrease in the tensile strength, flexural strength (except with NaOH and H_2O_2), and compressive strength and a very moderate increase in the impact strength of the BF/PE/MS biocomposites. The addition of ZnO nanorods and pretreatment of the banana fibers with NaOH, HCOOH, H_2O_2, Ac_2O, and $KMnO_4$ together enhanced all of the mechanical properties in the BF/PE/MS + ZnO nanobiocomposites substantially. HCOOH-, H_2O_2-, Ac_2O-, and $KMnO_4$-treated BF/PE/MS biocomposites have higher moisture absorption than the biocomposites with untreated fibers. But all of the nanobiocomposites containing ZnO nanorods show much lower water absorption. Our results suggest that the NaOH, HCOOH, and H_2O_2 treatments along with ZnO nanorods give superior materials.

5. MATERIALS AND METHODS

5.1. Chemical Treatments of Banana Fiber. *5.1.1. Alkali Treatment.* Raw banana fibers were immersed in 5% aqueous NaOH solution at 25 °C for 2 h. The treated fibers were then washed three times with running water to remove excess of NaOH on the fibers. The fibers were then washed with 5% solution of glacial acetic acid in water to neutralize the traces of NaOH remaining on the fiber surface. The neutralized fibers were washed again with distilled water to remove the excess acetic anhydride. The rinsed banana fibers were dried in sunlight for 1 day.

5.1.2. Acetic Anhydride Treatment. The natural untreated banana fibers were dipped in 10% acetic anhydride in acetone for 2 h; the fibers were washed thrice with running water gently. The treated banana fibers were rinsed with distilled water and dried in sunlight for 1 day.

5.1.3. Hydrogen Peroxide Treatment. The unmodified raw banana fibers were soaked in 10% hydrogen peroxide solution in water for 2 h; the fibers were washed with tap water vigorously. The treated banana fibers were rinsed with distilled water three times and dried at room temperature for 24 h.

5.1.4. Formic Acid Treatment. The chopped banana fibers were soaked in 10% formic acid solution in water for 2 h; the soaked fibers were washed with tap water three times. Then, the treated fibers were rinsed with distilled water to remove the excess of formic acid and dried in sunlight for 1 day.

5.1.5. Permanganate Treatment. The banana fibers were soaked in 0.05 N $KMnO_4$ solution (water/acetone mixture in the ratio of 9:1) for 1 h; the treated fibers were washed with running water three times. The treated fibers were rinsed with distilled water and dried in air for 1 day.

5.2. Synthesis of ZnO Nanorods. ZnO nanorods were synthesized by the sol−gel method. Zinc sulfate (100 g, 0.3477 mol; $ZnSO_4 \cdot 7H_2O$) as the precursor for zinc and triethanolamine (TEA, 15.8 mL, 0.12 mol) as the stabilizer were taken in a 1000 mL RB flask. DI water (150 mL) and ethanol (150 mL) were added to the above mixture and heated to 70 °C with stirring. A solution containing 100 g (2.5 mol) of sodium hydroxide in 100 mL of a 1:1 mixture of ethanol and water was then added dropwise slowly and maintained at this temperature overnight. The milky white precipitate formed was filtered, washed with methanol, and dried in an air oven at 80 °C for 5 h to get free-flowing ZnO nanorod powder. The schematic representation of the synthesis of ZnO nanorods using the sol−gel method is given in Figure 8.
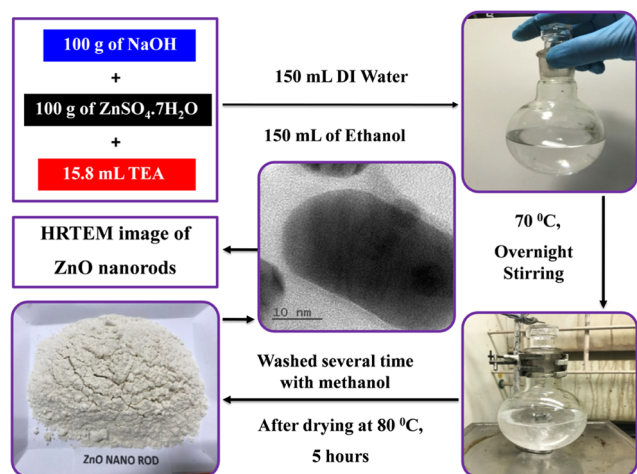
Figure 8. Schematic representation of the synthesis of ZnO nanorods.

5.3. Preparation of Hybrid Nanobiocomposites. The hybrid nanobiocomposites were prepared by the compression molding technique as shown in Figure 9 with the specimen dimensions of 290 mm × 290 mm × 3 mm. A thin layer of mold-releasing agent (PVA solution) was applied to the clean mold using a brush and allowed to dry. Meanwhile, 6 g of ZnO nanorods (2.4%) is synthesized in our laboratory as shown in Figure 1. Molecular sieves (30 g, 4 A^0; 12%) filler and acetone solvent (35 mL) were taken in a 500 mL beaker and stirred gently. Unsaturated polyester resin (200 g) was then added to this mixture, stirred using a mechanical stirrer for 30 min, and finally sonicated in a sonicator for 30 min. The excess of acetone solvent was removed by heating the mixture in a heating mantle at 80 °C for 10 min, cooled to room

temperature, 3 mL of the cobalt octoate solution (accelerator; 6% solution in styrene) was added, and stirred. Then, after 5 min, 3 mL of methyl ethyl ketone peroxide catalyst solution (6% solution in dimethyl phthalate) was added slowly and stirred well. To the above mixture, 100 g of short (2 cm long) banana fiber was added, mixed thoroughly using a glass rod, and poured on the mold. The mold was kept at a pressure of 1500 psi at room temperature for 30 min for curing and then post-cured at a temperature of 80 °C for 30 min. After curing, the composite samples were cut as per the ASTM standard.

5.3.1. Mechanical Testing. 5.3.1.1. Tensile Testing. The tensile tests of all of the hybrid biocomposites and nanobiocomposites were carried out according to the ASTM D 3089 standard, using a KALPAK Universal tester KIC-2-1000 (capacity 100 kN; model number SR.NO.12110) with a crosshead speed of 2 mm min^{-1} at room temperature. The dimensions of the specimen used for the test are 250 mm × 25 mm × 3 mm. Three samples were tested for each composition, and the average value was calculated. The ultimate tensile strength was calculated using the following formula

peak load/cross sectional area

= ultimate tensile strength (MPa)

5.3.2. Bending Test. The three-point bending test specimens (125 mm × 13 mm × 3 mm) of all of the hybrid biocomposites and nanobiocomposites were prepared as per ASTM D 790; the bending test was carried out using a KALPAK Universal tester KIC-2-1000 (capacity 100 kN; model number SR.NO.12110) with a crosshead speed of 2 mm min^{-1} at room temperature. Three samples were tested for each composition, and the average value was calculated. The load−displacement curve was obtained. Flexural strength (MPa) was calculated by the software.

5.3.3. Compressive Strength. Compressive tests of all of the hybrid biocomposites and nanobiocomposites were carried out as per the standard ASTM D 3410 (specimen dimensions: 150 mm × 25 mm × 3 mm) using a KALPAK Universal tester KIC-2-1000 (capacity 100 kN; model number SR.NO.12110) with a crosshead speed of 2 mm min^{-1} at room temperature. Three samples were tested, and the average value of the compressive strength was calculated from the stress−strain curve by the software.

5.3.4. Impact Strength. Izod impact test specimens (65 mm × 13 mm × 3 mm) of all of the hybrid biocomposites and nanobiocomposites were prepared according to ASTM D 256; an indigeneous Impact test machine (25J developed by Central Institute of Plastics Engineering and Technology (CIPET) Chennai, Tamilnadu, India) with a striking pendulum was used to determine the notched Izod impact strength. Three samples were tested for each composition, and the average value of the impact strength (J m^{-1}) was calculated.

impact energy (J)/thickness of the specimen (m)

= Izod impact strength (J m^{-1})

5.3.5. Water Absorption Test. The test specimens (20 mm × 20 mm × 3 mm) of all of the hybrid biocomposites and nanobiocomposites, prepared according to ASTM D 5229 and weighed (W_1), were kept immersed in water for 48 h at room temperature. Then, the specimens were taken out and the water adhering to the surface was wiped out using a dry tissue

Figure 9. Preparation of NaOH-treated randomly oriented short BF/PE/MS/ZnO hybrid nanobiocomposite by the compression molding technique.

paper and weighed (W_2). The percentage of water absorption was calculated using the formula

$$\% \text{ of water absorption} = (W_2 - W_1)/(W_1) \times 100$$

Three samples were tested, and the average value was obtained.

■ AUTHOR INFORMATION

Corresponding Author

   Sarojadevi Muthusamy − *Department of Chemistry, Anna University, Chennai 600025, India*; Email: msrde2000@yahoo.com

Authors

   Chinnappa Arumugam − *Department of Chemistry, Anna University, Chennai 600025, India*
   Gandarvakottai Senthilkumar Arumugam − *National Center for Flexible Electronics, IIT Kanpur, Kanpur 208016, India*
   Ashok Ganesan − *Metabolic Engineering Group, ICGEB, New Delhi 110067, India*

Complete contact information is available at:
https://pubs.acs.org/10.1021/acsomega.1c02662

Author Contributions

S.M. contributed to supervision, methodology, and manuscript writing. C.A. contributed to the concept, experimental design, data analysis, and manuscript writing. G.S.A. contributed to the concept, experimental design, data analysis, and manuscript writing. A.G. contributed to the experimental design, technical editing, and manuscript writing. The manuscript was written through contributions of all authors. All authors have given approval to the final version of the manuscript.

Notes

The authors declare no competing financial interest.

■ ACKNOWLEDGMENTS

■ REFERENCES

(1) Pickering, K. L.; Efendy, M. G. A.; Le, T. M. A review of recent developments in natural fibre composites and their mechanical performance. *Composites, Part A* **2016**, *83*, 98−112.

(2) Cao, Y.; Chan, F.; Chui, Y. H.; Xiao, H. Characterization of flax fibres modified by alkaline, enzyme, and steam-heat treatments. *BioResources* **2012**, *7*, 4109−4121.

(3) Joseph, P. V.; Marcelo, S.; Rabello, L. H. C.; et al. Environmental Effects on the Degradation Behaviour of Sisal Fibre Reinforced Polypropylene Composites. *Compos. Sci. Technol.* **2002**, *62*, 1357−1372.

(4) Dhakal, H. N.; Zhang, Z. Y.; Richardson, M. O. W. Effect of Water Absorption on the Mechanical Properties of Hemp Fibre Reinforced Unsaturated Polyester Composites. *Compos. Sci. Technol.* **2007**, *67*, 1674−1683.

(5) Paul, S. A.; Boudenne, A.; Ibos, L.; Candau, Y.; Joseph, K.; Thomas, S. Effect of Fiber Loading and Chemical Treatments on

Thermophysical Properties of Banana Fiber/Polypropylene Commingled Composite Materials. *Composites, Part A* **2008**, *39*, 1582−1588.

(6) Sutharson, B.; Rajendran, M.; Devadasan, S. R.; Selvam, B. Effect of Chemical Treatments on Mechanical Properties of Jute Fiber Hybrid Composite Laminates. *ARPN J. Eng. Appl. Sci.* **2012**, *7*, 760−765.

(7) Herrera-Franco, P. J.; Valadez-González, A. A Study of the Mechanical Properties of Short Natural-Fiber Reinforced Composites. *Composites, Part B* **2005**, *36*, 597−608.

(8) Bledzki, A. K.; Gassan, J. Composites Reinforced with Cellulose Based Fibres. *Prog. Polym. Sci.* **1999**, *24*, 221−274.

(9) Venkateshappa, S. C.; Beerhall, B.; Kenchappa, M. G.; Ranganagowda, R. P. G. Flexural behaviour of areca fibres composites. *BioResources* **2010**, *5*, 1846−1858.

(10) Kumar, K. S.; Siva, I.; Rajini, N.; Jeyaraj, P.; Jappes, J. W. Tensile, impact, and vibration properties of coconut sheath/sisal hybrid composites: Effect of stacking sequence. *J. Reinf. Plast. Compos.* **2014**, *33*, 1802−1812.

(11) Atiqah, A.; Jawaid, M.; Ishak, M. R.; Sapuan, S. M. Effect of Alkali and Silane Treatments on Mechanical and Interfacial Bonding Strength of Sugar Palm Fibres with Thermoplastic Polyurethane. *J. Nat. Fibres* **2018**, *15*, 251−261.

(12) *Developments in Fiber- Reinforced Polymer (FRP) Composites for Civil Engineering*; Uddin, N., Ed.; Elsivier, 2013.

(13) Kabir, M. M.; Wang, H.; Lau, K. T.; Cardona, F. Chemical treatments on plant-based natural fibre reinforced polymer composites: An overview. *Composites, Part B* **2012**, *43*, 2883−2892.

(14) Yan, L.; Chouw, N.; Jayaraman, K. Flax fibre and its composites—a review. *Composites, Part B* **2014**, *56*, 296−317.

(15) Thakur, V. K.; Thakur, M. K. Processing and characterization of natural cellulose fibers/thermoset polymer composites. *Carbohydr. Polym.* **2014**, *109*, 102−117.

(16) Borba, P. M.; Tedesco, A.; Lenz, D. M. Effect of reinforcement nanoparticles addition on mechanical properties of SBS/Curauáfiber composites. *Mater. Res.* **2014**, *17*, 412−419.

(17) Saba, N.; Tahir, P.; Jawaid, M. A review on potentiality of nano filler/natural fiber filled polymer hybrid composites. *Polymers* **2014**, *6*, 2247−2273.

(18) Gururaja, M. N.; Hari Rao, A. N. A review on recent applications and future prospectus of hybrid composites. *Int. J. Soft. Comput. Eng.* **2012**, *1*, 352−355.

(19) Hossen, M. F.; Hamdan, S.; Rahman, M. R.; Rahman, M. M.; Liew, F. K.; Lai, J. C. Effect of fiber treatment and nanoclay on the tensile properties of jute fiber reinforced polyethylene/clay nanocomposites. *Fibers Polym.* **2015**, *16*, 479−485.

(20) Camargo, P. H. C.; Satyanarayana, K. G.; Wypych, F. Nanocomposites: synthesis, structure, properties and new application opportunities. *Mater. Res.* **2009**, *12*, 1−39.

(21) Dey, A.; Bajpai, O. P.; Sikder, A. K.; Chattopadhyay, S.; Khan, M. A. S. Recent advances in CNT/graphene based thermoelectric polymer nanocomposite: a proficient move towards waste energy harvesting. *Renewable Sustainable Energy Rev.* **2016**, *53*, 653−671.

(22) Devnani, G. L.; Sinha, S. Effect of nanofillers on the properties of natural fiber reinforced polymer composites. *Mater. Today Proc.* **2019**, *18*, 647−654.

(23) Shalwan, A.; Yousif, B. F. Influence of date palm fibre and graphite filler on mechanical and wear characteristics of epoxy composites. *Mater. Des.* **2014**, *59*, 264−273.

(24) Kuilla, T.; Bhadra, S.; Yao, D.; Kim, N. H.; Bose, S.; Lee, J. H. Recent advances in graphene based polymer composites. *Prog. Polym. Sci.* **2010**, *35*, 1350−1375.

(25) Potts, J. R.; Dreyer, D. R.; Bielawski, C. W.; Ruoff, R. S. Graphene-based polymer nanocomposites. *Polymer* **2011**, *52*, 5−25.

(26) Aziz, S. H.; Ansell, M. P. The effect of alkalinisation and fibre alignment on the mechanical and thermal properties of kenaf and hemp bast fibre composites: Part 1- polyester resin matrix. *Compos. Sci. Technol.* **2004**, *64*, 1219−1230.

(27) Faruk, O.; Bledzki, A. K.; Fink, H.-P.; Sain, M. Biocomposites reinforced with natural fibers: 2000−2010. *Prog. Polym. Sci.* **2012**, *37*, 1552−1596.

(28) Sapuan, S.; Leenie, A.; Harimi, M.; Beng, Y. Mechanical properties of woven banana fibre reinforced epoxy composites. *Mater. Des.* **2006**, *27*, 689−693.

(29) Mohan Rao, K. M.; Mohan Rao, K. Extraction and tensile properties of natural fibers;Vakka, date and bamboo. *Compos. Struct.* **2007**, *77*, 288−295.

(30) Mohan, T. P.; Kanny, K. Water barrier properties of nanoclay filled sisal fibre reinforced epoxy composites. *Composites, Part A* **2011**, *42*, 385−393.

(31) Meulenkamp, E. A. Synthesis and Growth of ZnO Nanoparticles. *J. Phys. Chem. B* **1998**, *102*, 5566−5572.

(32) Spanhel, L.; Anderson, M. A. Semiconductor Cluster in the Sol-Gel Process: Quantized Aggregation, Gelation, and Crystal Growth in Concentrated ZnO colloids. *J. Am. Chem. Soc.* **1991**, *113*, 2826−2833.

(33) Koao, L. F.; Dejene, F. B.; Swart, H. C. Properties of flower-like ZnO nanostructures synthesized using the chemical bath deposition. *Mater. Sci. Semicond. Process.* **2014**, *27*, 33−40.

(34) Jiang, L.; Li, G.; Ji, Q.; Peng, H. Morphological control of flower-like ZnO nanostructures. *Mater. Lett.* **2007**, *61*, 1964−1967.

(35) Visinescu, D.; DyiaHussien, M.; Moreno, J. C.; Negrea, R.; Birjega, R.; Somacescu, S.; Cristian, D. E.; Chifiriuc, M. C.; Popa, M.; Miruna, S.; Stan, O. C. Zinc Oxide Spherical-Shaped Nanostructures: Investigation of Surface Reactivity and Interactions with Microbial and Mammalian Cells. *Langmuir* **2018**, *34*, 13638−13651.

(36) Noman, M. T.; Petru, M.; Militky, J.; Azeem, M.; Ashraf, M. A. Sonochemical Synthesis of ZnO Nanoparticles for Photocatalytic Applications, Modelling and Optimization. *Materials* **2020**, *13*, No. 14.

(37) Govender, K.; Boyle, D. S.; Kenway, P. B.; O'Brien, P. Understanding the factors that govern the deposition and morphology of thin films of ZnO from aqueous solution. *J. Mater. Chem.* **2004**, *14*, 2575−2591.

(38) Top, A.; Çetinkaya, H. Zinc oxide and zinc hydroxide formation via aqueous precipitation: Effect of the preparation route and lysozyme addition. *Mater. Chem. Phys.* **2015**, *167*, 77−87.

(39) Trindade, T.; de Jesus, J. D. P.; O'Brien, P. Preparation of zinc oxide and zinc sulfide powders by controlled precipitation from aqueous solution. *J. Mater. Chem.* **1994**, *4*, 1611−1617.

(40) Haque, M. A.; Mahalakshm, S. Effect of Triethanolamine on Zinc Oxide Nanoparticles. *Mater. Focus* **2013**, *2*, 469−474.

(41) Ban, T.; Sakai, T.; Ohya, Y. Synthesis of zinc oxide crystals with different shapes from zincate aqueous solutions stabilized with Triethanolamine. *Cryst. Res. Technol.* **2007**, *42*, 849−855.

(42) Ahmed, M. T.; Abd-Elhamid, M. I.; Sarhan, A.; Hassan, A. Preparation and Characterization of ZnO Nanoparticles by Simple Precipitation Method. *Int. J. Sci., Eng. Technol.* **2016**, *4*, 507.

(43) Koutu, V.; Shastri, L.; Malik, M. M. Effect of NaOH concentration on optical properties of zinc oxide nanoparticles. *Mater. Sci.-Pol.* **2016**, *34*, 819−827.

(44) Xu, S.; Wang, Z. L. One-Dimensional ZnO Nanostructures: Solution Growth and Functional Properties. *Nano Res* **2011**, *4*, 1013−1098.

(45) Umar, A.; Hahn, Y. B. ZnO Nanoparticles: Growth, Properties, and Applications. In *Metal Oxide Nanostructures and Their Applications*; Umar, A.; Hahn, Y. B., Eds.; American Scientific Publishers: California, 2010; p 1.

(46) Polsongkram, D.; Chamninok, P.; Pukird, S.; Chow, L.; Lupan, O.; Chai, G.; Khallaf, H.; Park, S.; Schulte, A. Effect of synthesis conditions on the growth of ZnO nanorods via hydrothermal method. *Phys. B* **2008**, *403*, 3713.

(47) Chun, S. M.; Choi, D. H.; Park, J. B.; Hong, Y. C. Optical and Structural Properties of ZnO Nanoparticles Synthesized by CO_2 Microwave Plasma at Atmospheric Pressure. *J. Nanopart.* **2014**, No. 734256.

(48) Lavand, A. B.; Malghe, Y. S. Synthesis, characterization and visible light photocatalytic activity of nitrogen-doped zinc oxide nanospheres. *J. Asian Ceram. Soc.* **2015**, *3*, 305−310.

(49) Fakhari, S.; Jamzad, M.; KabiriFard, H. Green synthesis of zinc oxide nanoparticles: a comparison. *Green Chem. Lett. Rev.* **2019**, *12*, 19−24.

(50) Alwan, R. M.; Kadhim, Q. A.; Sahan, K. M.; Ali, R. A.; Mahdi, R. J.; Kassim, N. A.; Jassim, A. N. Synthesis of Zinc Oxide Nanoparticles via Sol − Gel Route and Their Characterization. *Nanosci. Nanotechnol.* **2015**, *5*, 1−6.

(51) Jay Chithra, M.; Sathya, M.; Pushpanathan, K. Effect of pH on Crystal Size and Photoluminescence Property of ZnO Nanoparticles Prepared by Chemical Precipitation Method. *Acta Metall. Sin.* **2015**, *28*, 394−404.

(52) Stan, M.; Popa, A.; Toloman, D.; Silipas, T.-D.; Vodnar, D. C. Antibacterial and Antioxidant Activities of ZnO Nanoparticles Synthesized Using Extracts of Allium sativum, Rosmarinus officinalis and Ocimumbasilicum. *Acta Metall. Sin.* **2016**, *29*, 228−236.

(53) Soni, B. H.; Deshpande, M. P.; Bhatt, S. V.; Garg, N.; Chaki, S. H. Studies on ZnO Nanorods Synthesized by Hydrothermal Method and their Characterization. *J. Nano- Electron. Phys.* **2013**, *5*, 6.

(54) Šarić, A.; Music, S.; Ivanda, M. Varying the microstructural properties of ZnO particles using different synthesis routes. *J. Mol. Struct.* **2011**, *993*, 219−224.

(55) Andrés-Vergés, M.; Mifsud, A.; Serna, C. J. Formation of rod-like zinc oxide microcrystals in homogeneous solutions. *J. Chem. Soc. Faraday Trans.* **1990**, *86*, 959.

(56) Handore, K.; Bhavsar, S.; Horne, A.; Chhattise, P.; Mohite, K.; Ambekar, J.; Pande, N.; Chabukswar, V. Novel Green Route of Synthesis of ZnO Nanoparticlesby Using Natural Biodegradable Polymer and Its Application as a Catalyst for Oxidation of Aldehydes. *J. Macromol. Sci., Part A: Pure Appl.Chem.* **2014**, *51*, 941−947.

(57) Singh, J.; Kaur, S.; Kaur, G.; Basuand, S.; Rawat, M. BiogenicZnO nanoparticles: a study of blueshift of optical band gap and photocatalytic degradation of reactive yellow 186 dye under direct sunlight. *Green Process. Synth.* **2019**, *8*, 272−280.

(58) Yedurkar, S.; Maurya, C.; Mahanwar, P. Biosynthesis of Zinc OxideNanoparticles Using Ixora CoccineaLeaf Extract—A Green Approach. *Open J. Synth. Theory Appl.* **2016**, *5*, 1−14.

(59) Kumar, H.; Rani, R. Structural and Optical Characterization of ZnO Nanoparticles Synthesized by Microemulsion Route. *Int. Lett. Chem., Phys. Astron.* **2013**, *19*, 26−36.

(60) Omri, K.; Najeh, I.; Dhahri, R.; El Ghoul, J.; El Mir, L. Effects of temperature on the optical and electrical properties of ZnO nanoparticles synthesized by sol−gel method. *Microelectron. Eng.* **2014**, *128*, 53−58.

(61) Arora, A. K.; Devi, S.; VheelJaswal, V.; Singh, J.; Minger, M.; Gupta, V. D. Synthesis and Characterization of ZnO Nanoparticles. *Orient. J. Chem.* **2014**, *30*, 1671−1679.

(62) Kołodziejczak-Radzimska, A.; Markiewicz, E.; Jesionowski, T. StructuralCharacterisation of ZnO Particles Obtained by the Emulsion Precipitation Method. *J. Nanomater.* **2012**, No. 656353.

(63) Hasnidawani, J. N.; Azlina, H. N.; Norita, H.; Bonnia, N. N.; Ratim, S.; Ali, E. S. Synthesis of ZnO nanostructures using sol − gel method. *Procedia Chem.* **2016**, *19*, 211−216.

(64) Osman, D. A. M.; Mustafa, M. A. Synthesis and Characterization of Zinc Oxide Nanoparticles using Zinc Acetate Dihydrate and Sodium Hydroxide. *J. Nanosci. Nanoeng.* **2015**, *1*, 248−251.

(65) Shamhari, N. M.; Wee, B. S.; Chin, S. F.; Kok, K. Y. Synthesis and Characterization of Zinc Oxide Nanoparticles with Small Particle Size Distribution. *Acta Chim. Slovaca* **2018**, *65*, 578−585.

(66) Shah, H.; Srinivasulu, B.; Shit, S. C. Influence of Banana Fibre Chemical Modi cation on the Mechanical and Morphological Properties of Woven Banana Fabric /Unsaturated Polyester Resin Composites. *Polym. Renewable Res.* **2013**, *4*, 61−84.

(67) Sreekala, M. S.; Thomas, S. Effect of fiber surface modification on water-sorption characteristics of oil palm fibers. *Compos. Sci. Technol.* **2003**, *63*, 861−86.

(68) Gonçalves, A. P. B.; de Miranda, C. S.; Guimarães, D. H.; de Oliveira, J. C.; Cruz, A. M. F.; da Silva, F. L. B. M.; Luporini, S.; MamedeJose, N. Physicochemical, Mechanical and Morphologic Characterization of Purple Banana Fibers. *Mater. Res.* **2015**, *18*, 205−209.

(69) Bessadok, A.; Marais, S.; Gouanv'e, F.; Colasse, L.; Zimmerlin, I.; Roudesli, S.; M'etayer, M. Effect of chemical treatments of Alfa (Stipa tenacissima) fibres on water sorption properties. *Compos. Sci. Technol.* **2007**, *67*, 685−697.

(70) Ndazi, B. S.; et al. Chemical and physical modifications of rice husks for use as composite panels. *Composites, Part A* **2007**, *38*, 925−935.

(71) Martin, A. R.; et al. Studies on the thermal properties of sisal fiber and its constituents. *Thermochim. Acta* **2010**, *506*, 14−19.

(72) Nabinejad, O.; Sujan, D.; Rahman, M. E.; Davies, I. J. Effect of oil palm shell powder on the mechanical performance and thermal stability of polyester composites. *Mater. Des.* **2015**, *65*, 823−830.

(73) (a) Nabinejad, O.; et al. Determination of filler content for natural filler polymer composite by thermogravimetric analysis. *J. Therm. Anal. Calorim.* **2015**, *122*, 227−233. (b) Indira, K. N.; Jyotishkumar, P.; Thomas, S. Thermal Stability and Degradation of Banana Fibre/PF Composites Fabricated by RTM. *Fibers Polym.* **2012**, *13*, 1319−1325.

(74) Alvarez, V. A.; Vazquez, A. Influence of fibre chemical modification procedure on the mechanical properties and water absorption of MaterBi-Y/sisal fibre composites. *Composites, Part A* **2006**, *37*, 1672−80.

(75) Benıtez, A. N.; Monzon, M. D.; Angulo, I.; Ortega, Z.; Hernandez, P. M.; Marrero, M. D. Treatment of banana fiber for use in the reinforcement of polymeric matrices. *Measurement* **2013**, *46*, 1065−73.

(76) Arumugam, C.; Arumugam, S.; Muthusamy, S. Mechanical, thermal and morphological properties of unsaturated polyester/ chemically treated woven kenaf fiber/AgNPs@PVA hybrid nano-biocomposites for automotive applications. *J. Mater. Res. Technol.* **2020**, *9*, 15298−15312.

(77) Allysa Gabrielle, N. B.; Llanos, P. S. P.; de Yro, P. A. N.; Sanglay, G. C. D.; Magdaluyo, E. R., Jr. Surface modification of abaca fibers by permanganate and alkaline treatment via factorial design. *AIP Conf. Proc.* **2019**, *2083*, No. 03000.

(78) Li, X.; Lope, G.; Tabil, S. P. Chemical Treatments of Natural Fiber for Use in Natural Fiber-Reinforced Composites: A Review. *J. Polym. Environ.* **2007**, *15*, 25−33.

(79) Sumesh, K. R.; Kandavel, K. Green Synthesis of Aluminium Oxide Nanoparticles and its Applications in Mechanical and Thermal Stability of Hybrid Natural Composites. *J. Polym. Environ.* **2019**, *27*, 2189−2200.

(80) Islam, M. S.; Ahmad, M. B.; Hasan, M.; Aziz, S. A.; Jawaid, M.; Haafiz, M.; Siti Zakaria, A. H. Natural Fiber-Reinforced Hybrid Polymer Nanocomposites: Effect of Fiber Mixing and Nanoclay on Physical, Mechanical and Biodegradable Properties. *BioResources* **2014**, *10*, 1394−1407.

(81) Borba, P. M.; Tedesco, A.; Lenz, D. M. Effect of reinforcement nanoparticles addition on mechanical properties of SBS/Curauáfiber composites. *Mater. Res.* **2014**, *17*, 412−419.

(82) Sharba, M. J.; Leman, Z.; Sultan, M. T. H.; Ishak, M. R.; Hanim, M. A. Z. Tensile and Compressive Properties of Woven Kenaf/Glass Sandwich Hybrid Composites. *Int. J. Polym. Sci.* **2016**, No. 1235048.

(83) Herrera-Estrada, L.; Pillay, S.; Vaidya, U. In *Banana Fiber Composites for Automotive and Transportation Applications*, 8th Annual SPE Automotive Composites, Conference and Exhibition, 2008.

(84) Bessadok, A.; Marais, S.; Roudesli, S.; Lixon, C.; Metayer, M. Influence of chemical modifications on water sorption and mechanical properties of Agave fibers. *Composites, Part A* **2008**, *39*, 29−45.

(85) Mohan, T. P.; Kanny, K. Compressive characteristics of unmodified and nanoclay treated banana fiber reinforced epoxy composite cylinders. *Composites, Part B* **2019**, *169*, 118−125.

(86) Rokbi, M.; Osmani, H.; Imad, A.; Benseddiq, N. Effect of Chemical treatment on Flexure Properties of Natural Fiber-reinforced Polyester Composite. *Procedia Eng.* **2011**, *10*, 2092−2097.

(87) Goriparthi, B. K.; Suman, K. N. S.; Mohan Rao, N. Effect of fiber surface treatments on mechanical and abrasive wear performance of polylactide/jute composites. *Composites, Part A* **2012**, *43*, 1800−1808.

(88) Rozman, H. D.; Rozyanty, A. R.; Musa, L.; Tay, G. S. Ultra-violet radiation-cured biofiber composites from kenaf: The effect of montmorillonite on the flexural and impact properties. *J. Wood Chem. Technol.* **2010**, *30*, 152−163.

(89) Sumesh, K. R.; Kanthavel, K. A.; Ajithram; Nandhini, P. Bioalumina Nano Powder Extraction and its Applications for Sisal, Coir and Banana Hybrid Fiber Composites: Mechanical and Thermal Properties. *J. Polym. Environ.* **2019**, *27*, 2068−2077.

(90) Vivek, S.; Kanthavel, K. Effect of bagasse ash filled epoxy composites reinforced with hybrid plant fibres for mechanical and thermal properties. *Composites, Part B* **2019**, *160*, 170−176.

(91) Husseinsyah, S.; Mostapha, M. The Effect of Filler Content on preparation of Coconut Shell Filled Polyester Composites. *Malays. Polym. J.* **2011**, *6*, 87−97.

(92) Adhikari, J.; Biswas, B.; Chabri, S.; Bandyapadhyay, N. R.; Sawai, P.; Bhairab, C. M.; Sinha, A. Effect of functionalized metal oxides addition on the mechanical, thermal and swelling behaviour of polyester/jute composites. *Eng. Sci. Technol., Int. J.* **2017**, *20*, 760−774.

(93) Kusmono, H.; Hestiawan, J. The water absorption, mechanical and thermal properties of chemically treated woven fan palm reinforced polyester composites. *J. Mater. Res.Technol.* **2020**, *9*, 4410−4420.